Acta Crystallographica Section F
Structural Biology and Crystallization Communications
ISSN 1744-3091

Structure of ribose 5-phosphate isomerase from the probiotic bacterium *Lactobacillus salivarius* UCC118

Carina M. C. Lobley,[a] Pierre Aller,[a] Alice Douangamath,[a] Yamini Reddivari,[b] Mario Bumann,[c] Louise E. Bird,[b] Joanne E. Nettleship,[b] Jose Brandao-Neto,[a] Raymond J. Owens,[b] Paul W. O'Toole[d] and Martin A. Walsh[a,c]*

[a]Diamond Light Source, Harwell Science and Innovation Campus, Didcot, Oxfordshire OX11 0DE, England, [b]Oxford Protein Production Facility UK, Research Complex at Harwell, R92 Rutherford Appleton Laboratories, Harwell, Oxfordshire OX11 0FA, England, [c]MRC France, BM14, c/o ESRF, 6 Rue Jules Horowitz, BP 220, 38043 Grenoble France, and [d]Department of Microbiology, Alimentary Pharmabiotic Centre, University College Cork, Cork, Ireland

Correspondence e-mail: martin.walsh@diamond.ac.uk

Received 22 August 2012
Accepted 12 October 2012

PDB Reference: ribose 5-phosphate isomerase, 4gmk

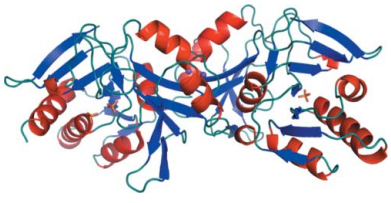

The structure of ribose 5-phosphate isomerase from the probiotic bacterium *Lactobacillus salivarius* UCC188 has been determined at 1.72 Å resolution. The structure was solved by molecular replacement, which identified the functional homodimer in the asymmetric unit. Despite only showing 57% sequence identity to its closest homologue, the structure adopted the typical α and β D-ribose 5-phosphate isomerase fold. Comparison to other related structures revealed high homology in the active site, allowing a model of the substrate-bound protein to be proposed. The determination of the structure was expedited by the use of *in situ* crystallization-plate screening on beamline I04-1 at Diamond Light Source to identify well diffracting protein crystals prior to routine cryocrystallography.

1. Introduction

Ribose 5-phosphate isomerase (EC 5.3.1.6; Rpi) is a key enzyme of the pentose phosphate pathway that catalyses the interconversion of ribose 5-phosphate (R5P) and ribulose 5-phosphate (Ru5P). It exists in two isoforms, RpiA and RpiB; although they catalyse the same reaction, they are evolutionarily distinct, sharing little sequence or structural homology. RpiA is widespread throughout all kingdoms of life, whereas RpiB is found in bacterial sources and some pathogenic eukaryotes. Rpi is involved in the synthesis of purine and pyrimidine nucleotides, NAD and amino acids, including histidine and tryptophan, by the production of R5P and in the synthesis of riboflavins *via* the precursor Ru5P (Hamada *et al.*, 2003; Zhang, Andersson, Savchenko *et al.*, 2003). In commensal bacteria such as lactobacilli, the pentose phosphate pathway provides an alternative to hexose metabolism, presumably because plant-derived ribose is common in the mammalian diet.

Structures of RpiA are known from a variety of organisms, including *Escherichia coli* (Rangarajan *et al.*, 2002; Zhang, Andersson, Savchenko *et al.*, 2003), *Pyrococcus horikoshii* (Ishikawa *et al.*, 2002), *Haemophilus influenzae* (PDB entry 1m0s; Northeast Structural Genomics Consortium, unpublished work), *Thermus thermophilus* (Hamada *et al.*, 2003), *Saccharomyces cerevisiae* (Graille *et al.*, 2005), *Plasmodium falciparum* (Holmes *et al.*, 2006), *Bartonella henselae* (PDB entry 3hhe; Seattle Structural Genomics Center for Infectious Disease, unpublished work), *Vibrio vulnificus* YJ016 (Kim *et al.*, 2009), *Methanocaldococcus jannaschii* (MJ1603; Strange *et al.*, 2009), *Francisella tularensis* (PDB entry 3kwm; Center for Structural Genomics of Infectious Diseases, unpublished work) and *Burkholderia thailandensis* (PDB entries 3uw1 and 3u7j; Seattle Structural Genomics Center for Infectious Disease, unpublished work). Fewer structures of RpiB are known, including those from *Thermatoga maritima* (Xu *et al.*, 2004), *E. coli* (Zhang, Andersson, Skarina *et al.*, 2003), *M. tuberculosis* (Roos *et al.*, 2004, 2005), *Clostridium thermocellum* (Jung *et al.*, 2011), *Streptococcus mutans* UA159 (PDB entry 3l7o; X.-X. Fan, K.-T. Wang & X.-D. Su, unpublished work), *Trypanosoma cruzi* (Stern *et al.*, 2011), *Coccidioides immitis* (Edwards *et al.*, 2011) and *Giardia lamblia* (PDB entry 3s5p; Seattle Structural Genomics Center for Infectious Disease, unpublished work).

Lactobacillus salivarius UC188 is a Gram-positive, probiotic, lactic acid bacterium which has been widely studied for its probiotic

Table 1
Data-collection and refinement statistics.

Values in parentheses are for the outermost shell.

Data collection	
X-ray source	I04-1, Diamond Light Source
Wavelength (Å)	0.917
Space group	*C*2
Unit-cell parameters (Å)	a = 129.32, b = 63.74, c = 59.84, α = 90, β = 107.6, γ = 90
Resolution (Å)	22–1.72 (1.76–1.72)
$R_{\rm merge}$†	0.066 (0.704)
$\langle I\rangle/\langle\sigma(I)\rangle$	17.3 (2.8)
Mosaicity (°)	0.2
Completeness (%)	99.2 (99.8)
Multiplicity	6.8 (6.8)
Refinement	
No. of reflections	331889 (24579)
No. of unique reflections	48927 (3613)
$R_{\rm cryst}$‡	0.17
$R_{\rm free}$‡	0.206
No. of atoms	
Protein	3574
Water	260
No. of phosphate ions	3
No. of potassium ions	2
Average B factors (Å^2)	
Protein	23.2
Phosphate (PO_4^{3-})	35.5
Potassium (K^+)	13.7
Waters	31.6
R.m.s. deviations	
Bond lengths (Å)	0.018
Bond angles (°)	1.93
Ramachandran statistics (%)	
Most favoured	98.9
Generously allowed	1.1
Disallowed	0
MolProbity all-atom clashscore	10.48

† $R_{\rm merge} = \sum_{hkl}\sum_i |I_i(hkl) - \langle I(hkl)\rangle| / \sum_{hkl}\sum_i I_i(hkl)$. ‡ $R_{\rm cryst} = \sum_{hkl} ||F_{\rm obs}| - |F_{\rm calc}|| / \sum_{hkl} |F_{\rm obs}|$, where $F_{\rm obs}$ and $F_{\rm calc}$ are the observed and calculated structure-factor amplitudes, respectively. $R_{\rm free}$ is calculated as for $R_{\rm cryst}$ but using a random 5% subset of the data excluded from the refinement.

benefits as it forms part of the microbiota of the gastrointestinal tract of humans. Research to date has shown that *L. salivarius* can confer health benefits including, but not limited to, prevention or hindrance of intestinal infections, the elimination of foodborne pathogens and reduction in inflammation and food intolerance (Corr *et al.*, 2007; Neville & O'Toole, 2010; O'Callaghan *et al.*, 2012). Here, we present the high-resolution crystal structure of RpiA from *L. salivarius*, which was solved as part of a structural proteomics project to shed further light on how *Lactobacilli* colonize and adapt to the local environment in the complex endogenous microbiota of the human gut.

2. Materials and methods

2.1. Protein production and crystallization

The full-length coding sequence for *L. salivarius* Rpi (LSL_1806) was cloned into pOPINF using the InFusion method described previously (Bird, 2011; Berrow *et al.*, 2007). The protein was produced in *E. coli* strain Rosetta pLysS (DE3) using the auto-induction method (Studier, 2005). The cells were harvested by centrifugation and frozen at 193 K (the yield of pure protein was 3 mg per litre). The purification protocol followed that described previously (Nichols *et al.*, 2009); briefly, defrosted cells were lysed and the soluble fraction was purified *via* nickel-chelation chromatography followed by gel-filtration chromatography. Protein-containing fractions were pooled and the N-terminal His_6 tag was removed using rhinovirus 3C protease followed by reverse purification using nickel-chelation chromatography. Purified protein was concentrated to 20 mg ml^{-1} in 20 m*M* Tris pH 7.5, 200 m*M* NaCl prior to crystallization.

Crystallization screening was carried out as published elsewhere (Walter *et al.*, 2005) and several conditions were identified, with crystals appearing after between 78 and 128 d incubation at 294 K.

2.2. *In situ* crystal screening and data collection

Ten crystal leads were identified in 96-well sparse-matrix screens from Emerald BioSystems (Wizard I and II) and Molecular Dimensions (Morpheus; Gorrec, 2009). X-ray diffraction of these initial crystal hits was screened using *in situ* plate screening on beamline I04-1 at Diamond Light Source. The setup currently in place at the beamline provides for up to four plates to be hosted in a plate hotel adjacent to the robot dewar in the experimental hutch. These plates were loaded by the CATS robotic arm (Ohana *et al.*, 2004) and inserted to intersect the X-ray beam at the standard sample position. The additional area required to sample the plate area of any standard Society for Biomolecular Sciences (SBS) 96-well plate in the beamline sample environment was generated by modification of the standard *xyz* alignment stage of the Maatel MD2 microdiffractometer. Specifically, the space envelope at the sample position in x and y has been augmented by increasing the translation range of the single ω axis by 100 mm and through changes under the goniometer to reclaim 50 mm.

Here, ten drops from two plates were screened using a 1 s exposure with a 50 µm^2 beam with an incident flux of 1.7×10^{11} photons s^{-1}. A rotation width of 4° was used to allow unequivocal distinction between salt and protein crystals. Diffraction data were collected on a PILATUS 2M detector. The total time for screening was of the order of an hour. The best crystal identified from the screening was obtained from condition No. 35 of the Wizard II screen from Emerald BioSystems, which consists of 800 m*M* sodium phosphate monobasic, 1.2 *M* potassium phosphate dibasic as the precipitant mixture in 0.1 *M* sodium acetate buffer. The crystals were cryoprotected directly in the crystallization drop by the addition of crystallization buffer containing 30% glycerol prior to flash-cooling in liquid nitrogen and the collection of diffraction data to a resolution of 1.72 Å. The data were processed automatically using *xia*2 (Winter, 2010; Evans, 2006; Leslie, 2006; Sauter *et al.*, 2004; Zhang *et al.*, 2006). Data-collection and reduction statistics are summarized in Table 1.

2.3. Structure determination and refinement

The crystal structure of *L. salivarius* Rpi was solved by molecular replacement using *MrBUMP* (Keegan & Winn, 2007; Murzin *et al.*, 1995; Pearson & Lipman, 1988). A solution was identified using *MOLREP* (Vagin & Teplyakov, 2010) with chain *A* of PDB entry 3enw (Kim *et al.*, 2009) prepared by *CHAINSAW* (Stein, 2008) as a model. The initial R factor of 52.3% was refined to $R_{\rm cryst}$ and $R_{\rm free}$ values of 36.8% and 41.6%, respectively, after 30 cycles of *REFMAC*5 (Murshudov *et al.*, 2011). The *ARP*/*wARP* web server (Evrard *et al.*, 2007) was used to autobuild the structure, which resulted in an almost completed model with $R_{\rm cryst}$ and $R_{\rm free}$ values of 19.8% and 24.3%, respectively. Subsequent manual model building and refinement with *Coot* (Emsley & Cowtan, 2004) and *REFMAC*5, respectively, which included the modelling of 21 amino-acid side chains with dual conformations, resulted in a final model with $R_{\rm cryst}$ and $R_{\rm free}$ values of 17.0% and 20.6%, respectively. The final model was validated by *MolProbity* (Chen *et al.*, 2010) and the *RCSB Validation Server* (Berman *et al.*, 2000, 2003). Refinement statistics are detailed in Table 1.

Table 2
Results of *in situ* screening of RpiA crystallization hit conditions.

Crystal screen	Well	Well solution	Outcome
Wizard I and II	A6	20% PEG 3000, 0.1 *M* citrate pH 5.5	Salt crystals
	A8	2.0 *M* ammonium sulfate, 0.1 *M* citrate pH 5.5	No diffraction
	G11	0.8 *M* sodium phosphate/1.2 *M* potassium phosphate, 0.1 *M* acetate pH 4.5	Strong diffraction to 2.7 Å resolution, easily indexed and subsequently used for data collection
Morpheus	A5	0.06 *M* Divalents Mix, 0.1 *M* Buffer System 2 pH 7.5, 30% PEG550MME_P20K Mix	No diffraction
	C1	0.09 *M* NPS Mix, 0.1 *M* Buffer System 1 pH 6.5, 30% PEG550MME_P20K Mix	Diffraction spots observed to 6 Å resolution
	D1	0.12 *M* Alcohols Mix, 0.1 *M* Buffer System 1 pH 6.5, 30% PEG550MME_P20K Mix	Diffraction spots observed to 6 Å resolution
	E1	0.12 *M* Ethylene Glycols Mix, 0.1 *M* Buffer System 1 pH 6.5, 30% PEG550MME_P20K Mix	Diffraction spots observed to 6.5 Å resolution
	G4	0.10 *M* Carboxylic Acids Mix, 0.1 *M* Buffer System 1 pH 6.5, 37.5% MPD_P1K_P3350 Mix	Highly mosaic diffraction with spots observed to 3 Å resolution (harvesting of crystals unsuccessful, no further characterization)
	H4	0.10 *M* Amino Acids Mix, 0.1 *M* Buffer System 1 pH 6.5, 37.5% MPD_P1K_P3350 Mix	Diffraction spots observed to 6 Å resolution
	H5	0.10 *M* Amino Acids Mix, 0.1 *M* Buffer System 2 pH 7.5, 30% PEG550MME_P20K Mix	Diffraction spots observed to 9 Å resolution

3. Results and discussion

3.1. Benefits of *in situ* crystal screening

In situ diffraction experiments were first reported in 2004 (Jacquamet *et al.*, 2004) and clearly illustrated the potential of the method for accelerating the crystal-to-structure turnaround time. However, these initial experiments were compromised somewhat by the crystallization-plate geometry and the significant scattering from the plate plastic. Although an integrated X-ray system for the home laboratory (the PX scanner from Agilent) has been available for some time, the true potential of the method is now being realised, with a number of synchrotron beamlines enabling the method to be routinely accessed by users, notably at the Swiss Light Source, where a dedicated facility has been implemented (Bingel-Erlenmeyer *et al.*, 2011), BM30 at the ESRF (Jacquamet *et al.*, 2009) and Diamond (Axford *et al.*, 2012). Moreover, the development of low X-ray scattering SBS-format crystallization plates (CrystalQuickX, Greiner Bio-One, Germany) has significantly increased the tractability of performing *in situ* data collections (le Maire *et al.*, 2011; Wang *et al.*,

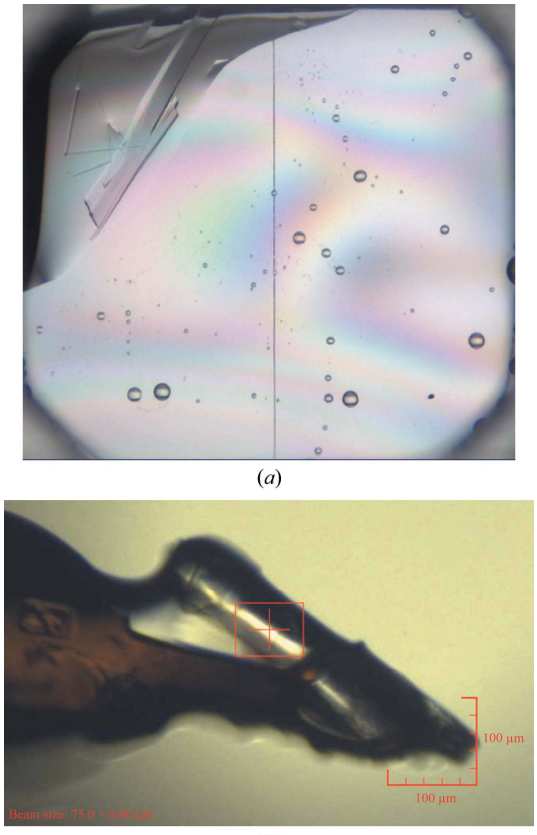

(*a*)

(*b*)

Figure 1
(*a*) Snapshot of the RpiA crystal in the 96-well plate before *in situ* screening. The plates were stored at 293 K and imaged using a Formulatrix Rock Imager. (*b*) An image captured from the I04-1 on-axis viewing system showing the same crystal mounted and cryoprotected at the beamline before data collection.

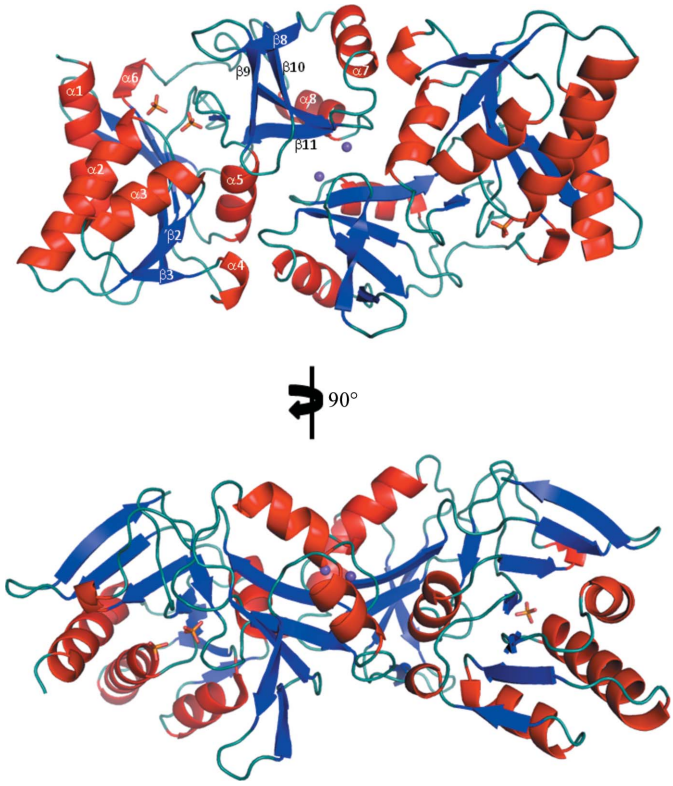

Figure 2
The overall dimeric structure of RpiA from *L. salivarius*, with each chain coloured by secondary structure (helices in red, β-strands in blue and random coils in teal). The two K^+ ions located at the dimer interface are shown as purple spheres and the three phosphate (PO_4^{3-}) ions are shown in stick representation: two in the active site of chain *A* and one in the active site of chain *B* (yellow sticks).

2012) and the development of other crystallization devices developed with *in situ* capabilities in mind should have an impact on the method (see Hargreaves, 2012 and references therein).

The recently commissioned *in situ* diffraction capability available on beamline I04-1 at Diamond Light Source provides an ideal facility for the rapid screening of crystal quality and subsequent standard data collection after crystal harvesting. Use of the CATS robot for handling the SBS standard plates allows the method to be integrated into the standard beamline setup, thus allowing the user to swap quickly between an *in situ* screening experiment and a standard data collection with a cryogenically cooled loop-mounted crystal using the Maatel MD2 diffractometer. The experiment workflow is accommodated within the beamline software control (*GDA* at Diamond; http://opengda.org), which provides an interface for the user to easily navigate to the crystallization wells containing crystal hits; the viewing system at low zoom levels is able to display a clear view of the crystallization well, allowing the user to quickly centre on the crystal of interest in the drop.

For the RpiA experiment, crystals were ranked based on the *in situ* diffraction experiment; ten crystallization conditions with crystal hits were screened directly *in situ*, which showed that although nine of the ten conditions contained protein crystals, only that in one condition (Fig. 1*a*) gave strong diffraction to beyond 3 Å resolution (Table 2). This crystal was then harvested and used to collect a 1.72 Å resolution data set immediately after the *in situ* experiment (Fig. 1*b*). As the crystallization condition for these crystals only yielded crystals after between 78 and 128 d, reproducing the crystals proved to be challenging. In this case crystal hits were effectively ranked by *in situ* screening, enabling the most effective use of the allocated beamtime, with data being collected immediately following the screening session

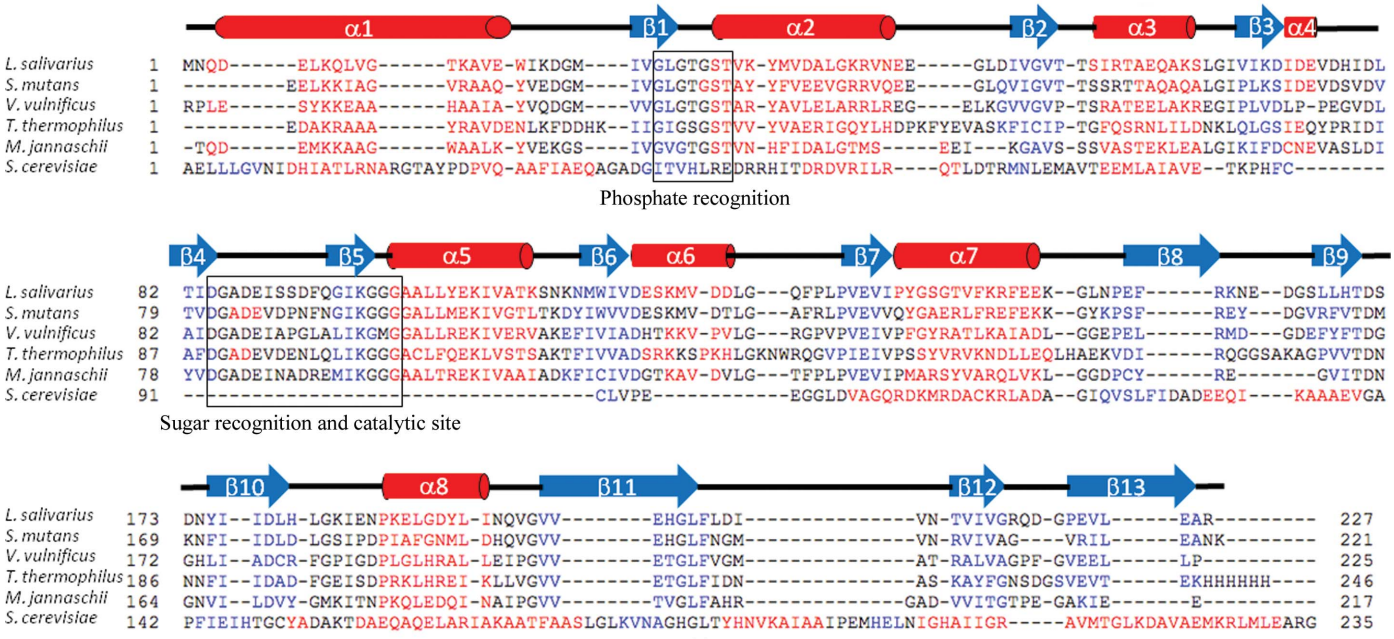

(*a*)

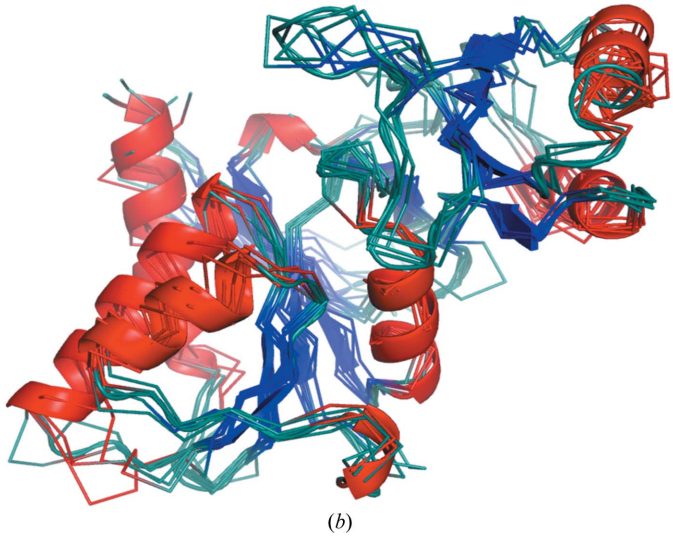

(*b*)

Figure 3
(*a*) Structure-based sequence alignment of the *L. salivarius* structure with the published structures with PDB codes 3l7o, 3enq (Kim *et al.*, 2009), 1uj4 (Hamada *et al.*, 2003), 3ixq (Strange *et al.*, 2009) and 1xtz (Graille *et al.*, 2005). (*b*) Superposed structures of one protomer from the above members of the RpiA family coloured as in Fig. 2. The *L. salivarius* structure is shown in cartoon representation. Molecular-graphics figures were all prepared using *PyMOL* (Schrödinger LLC). The sequence alignment was prepared in *PROMALS3D* (Pei *et al.*, 2008).

on the beamline from the best identified crystal. The changeover time from *in situ* screening to the standard data-collection setup at I04-1 is currently under 30 min. The process has been successfully repeated for two other projects and is proving to be highly effective for making the best use of the synchrotron beamtime available.

3.2. RpiA structure and comparison with the D-ribose-5-phosphate isomerase family

The overall topology of *L. salivarius* RpiA (Figs. 2 and 3) is broadly similar to other known RpiA structures. The N-terminal domain consists of α-helices 1–5 and β-strands 1–3, 6, 12 and 13. The C-terminal domain consists of α-helices 6 and 7 and β-strands 7–10. The remaining three β-strands form the interface between the two domains. In RpiA structures the domain interface typically consists of four β-strands. From a structural superposition (not shown) we see that the fourth strand, which would have been made by residues 124–126, is in fact an extended loop in the *L. salivarius* structure. While there is this very subtle change in topology, the extended loop occupies broadly the same position as the short β-strand that it replaces. The *L. salivarius* structure fits well into the SCOP α and β family of D-ribose-5-phosphate isomerase (RpiA) catalytic domains, as would be expected.

The structure presented contains a dimer in the asymmetric unit (Fig. 2). The two protomers in the asymmetric unit are highly similar, with a global r.m.s difference of 0.99 Å on superposition using *proSMART* (Nicholls, 2011). The presence of a dimer correlates with two observations on the protein in solution. Firstly, during gel-filtration chromatography to purify RpiA the protein eluted at a point corresponding to approximately the molecular weight of a dimer. Secondly, the purified protein was assessed using a Viscotek OmniSEC Tetra detector, which gave a molecular mass in solution of 44.388 kDa (dimer molecular weight of 49.74 kDa; data not shown). Analysis of the dimer interaction site using the *PISA* web server (Krissinel & Henrick, 2007; http://www.ebi.ac.uk/pdbe/prot_int/pistart.html) indicated that the dimer interface involves 33 amino acids from each protomer and buries an interface area of approximately 2167 Å^2. While there are no covalent bonds or salt bridges in the dimer interface, there are seven hydrogen bonds (involving residues Thr54, Asp74, Lys112, Tyr141, Ser143, Gly144 and Thr145 from both protomers) and numerous hydrophobic interactions stabilizing dimerization. This dimer interface is replicated across the RpiA family, where the biologically relevant dimer interfaces are comprised of predominantly hydrophobic interactions with a few key hydrogen bonds, although the dimer interface is only slightly more conserved than the surface residues. The role of the dimer in biological activity is unclear; each subunit presents an active site and there is no evidence for the dimer interface having a role in allosteric regulation (Zhang, Andersson, Savchenko *et al.*, 2003). Two crystallographic potassium ions complexed from the crystallization buffer have been modelled in the dimer interface. Each is coordinated by three protein residues, Ile195, Gln197 and Val200, and by three water molecules in extended water networks.

The active site is located in a shallow groove at the interface between the N-terminal and the C-terminal domains and is made up of two regions of conserved residues (Figs. 2 and 3*a*). The conserved sequence G*X*G(T/S)GST that is known to contain the phosphate-recognition sequence is $_{25}$GLGTGST$_{31}$ in *L. salivarius*. The second conserved region, DGADE(X)$_8$KGXG, which contains the sugar-recognition sequence and the catalytic residues, is $_{84}$DGADE(ISSDFQGI)KGGG$_{100}$ in *L. salivarius*. The crystals were grown in the absence of substrate, product or analogues. In some structures, the crystallization of apo RpiA has given rise to apo structures, including the *S. mutans* structure 3l7o, the *V. vulnificus* structure 3enq and the *E. coli* structure 1ks2. However, the structure presented here contains three phosphates, which are clearly visible in the electron density. Phosphate 1 is bound to the sugar-recognition sequence of protomer *A*, whilst phosphates 2 and 3 are bound to the phosphate-recognition pockets of protomer *A* and *B*, respectively (Fig. 4).

A close inspection of the active site of RpiA has been made focusing on three species: *L. salivarius*, *S. mutans* and *V. vulnificus*. *S. mutans* is phylogenetically close to the lactobacilli; it encodes the closest sequence homologue (57%) to the *L. salivarius* enzyme and is an apo structure. The enzyme from the more phylogenetically distant Gram-negative marine organism *V. vulnificus* has only 44% sequence

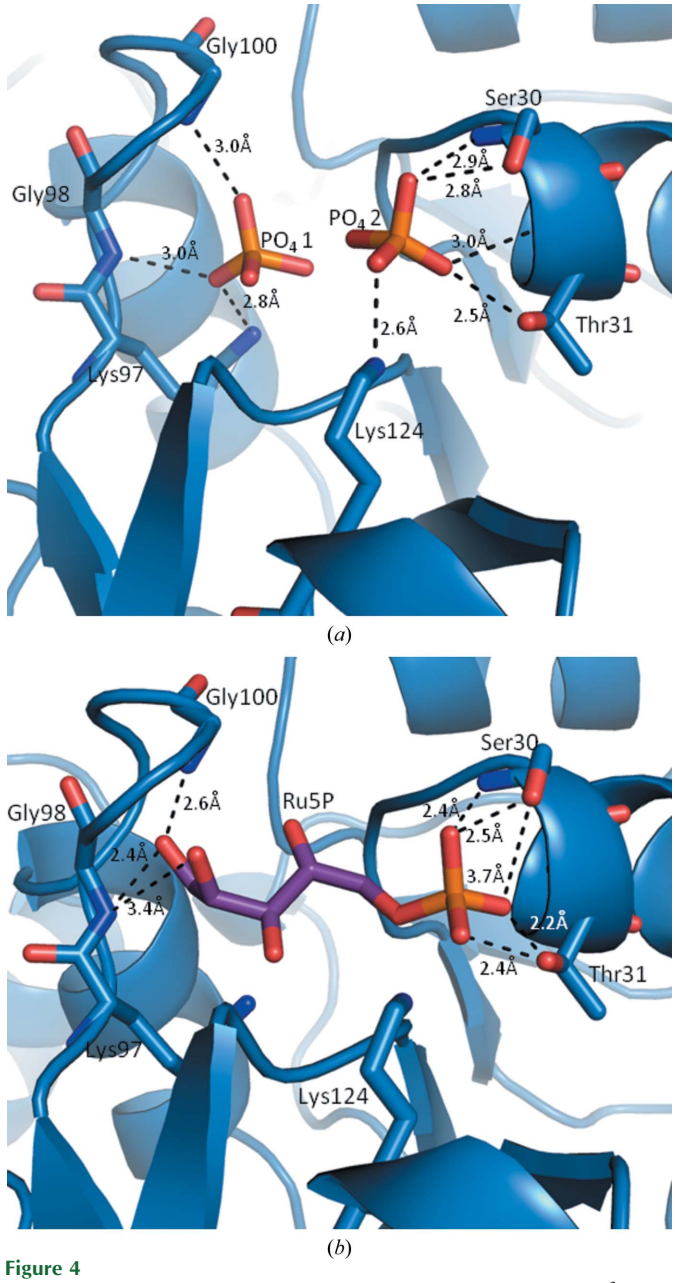

Figure 4
(*a*) The active site of *L. salivarius* RpiA showing the two phosphate (PO_4^{3-}) ions bound in the phosphate- and sugar-binding pockets. (*b*) Model of Ru5P bound to *L. salivarius* RpiA using the bound phosphate ions as a reference based on the structure of Ru5P bound to *V. vulnificus*, showing that the mode of binding is likely to be essentially identical.

Table 3
Structural superposition of RpiA structures.

Each chain was independently aligned and superposed on both chain *A* and chain *B* of the *L. salivarius* RpiA structure using *proSMART*. Results are shown for the comparison of chain *A*. Ru5P, ribulose 5-phosphate; A5P, arabinose-5-phosphate.

PDB code	Chain	Species	Ligands	Sequence identity (%)	Global r.m.s.d.† (Å)
4gmk	*A*	*L. salivarius* UCC118	PO_4^{3-}, K^+	100.0	—
	B			100.0	0.99
3l7o	*A*	*S. mutans* UA159	Apo	56.6	1.4
	B			57.4	0.7
3enq	*A*	*V. vulnificus* YJ016	Apo	44.4	1.6
	B			44.4	1.8
3env	*A*	*V. vulnificus* YJ016	A5P	44.4	1.8
	B			44.4	1.7
3enw	*A*	*V. vulnificus* YJ016	Ru5P	44.4	1.6
	B			44.4	1.7

† Global r.m.s.d. of main-chain atoms after superposition of all aligned residues based on aligned residues.

identity but has been solved as an apo structure, with the substrate Ru5P bound and with the inhibitor arabinose 5-phosphate bound. The structures from these three species superpose very closely, with only two minor side-chain differences in the active site. Firstly, at position 100 in *L. salivarius* and *S. mutans* there is a glycine residue which makes a hydrogen bond to phosphate 1. In *V. vulnificus* this is replaced by an alanine residue, which causes a change in the backbone conformation. Secondly, in the phosphate-binding region the *L. salivarius* structure has a hydrogen bond to the phosphate from Thr31. In the Ru5P-bound *V. vulnificus* structure this threonine occupies a different geometry and the hydrogen bond is made by Lys97 (Fig. 4). These two changes slightly extend the substrate-binding pocket, allowing it to easily accommodate the linear substrate molecule. The family of *V. vulnificus* structures demonstrate that binding of the substrate causes no perturbation of the active site. The substrate-bound *V. vulnificus* structure provides an excellent model for substrate binding in *L. salivarius* (Fig. 4*b*). In contrast, the inhibitor is predominantly solvent-exposed, with the sugar ring binding the phosphate-binding pocket and the phosphate group directed towards the solvent.

L. salivarius RpiA was compared with 20 known RpiA structures using *proSMART*, a structure-alignment tool that uses the conservation of local structure to produce a conformation-independent structural comparison of protein chains (Nicholls, 2011). This analysis showed that despite low sequence identity (26–57%) the global r.m.s. difference is indicative of close structural homology (0.7–2.0 Å; abbreviated data are given in Table 3 and Fig. 3). While the domain structure of RpiA is largely identical, conformational differences can be observed in the domain interface, causing subtle changes in the angle between the N-terminal and C-terminal domains. The other area in which the structures differ is in the extended loop connecting β-strands 8 and 9 (residues 160–175), where some flexibility can be inferred from the deviations in modelled positions across the 20 structures.

The authors thank Matthew Jenions for the Viscotek OmniSEC Tetra detector results. Initial work on this project was supported by a joint MRC/BBSRC grant to MAW. Work in the laboratory of PWO'T is supported by a Science Foundation Ireland grant to the Alimentary Pharmabiotic Centre and a Principal Investigator award. We thank Alimentary Health Ltd for providing strain UCC118.

References

Axford, D. *et al.* (2012). *Acta Cryst.* D**68**, 592–600.
Berman, H., Henrick, K. & Nakamura, H. (2003). *Nature Struct. Biol.* **10**, 980.
Berman, H. M., Westbrook, J., Feng, Z., Gilliland, G., Bhat, T. N., Weissig, H., Shindyalov, I. N. & Bourne, P. E. (2000). *Nucleic Acids Res.* **28**, 235–242.
Berrow, N. S., Alderton, D., Sainsbury, S., Nettleship, J., Assenberg, R., Rahman, N., Stuart, D. I. & Owens, R. J. (2007). *Nucleic Acids Res.* **35**, e45.
Bingel-Erlenmeyer, R., Olieric, V., Grimshaw, J. P. A., Gabadinho, J., Wang, X., Ebner, S. G., Isenegger, A., Schneider, R., Schneider, J., Glettig, W., Pradervand, C., Panepucci, E. H., Tomizaki, T., Wang, M. & Schulze-Briese, C. (2011). *Cryst. Growth Des.* **11**, 916–923.
Bird, L. E. (2011). *Methods*, **55**, 29–37.
Chen, V. B., Arendall, W. B., Headd, J. J., Keedy, D. A., Immormino, R. M., Kapral, G. J., Murray, L. W., Richardson, J. S. & Richardson, D. C. (2010). *Acta Cryst.* D**66**, 12–21.
Corr, S. C., Li, Y., Riedel, C. U., O'Toole, P. W., Hill, C. & Gahan, C. G. (2007). *Proc. Natl Acad. Sci. USA*, **104**, 7617–7621.
Edwards, T. E., Abramov, A. B., Smith, E. R., Baydo, R. O., Leonard, J. T., Leibly, D. J., Thompkins, K. B., Clifton, M. C., Gardberg, A. S., Staker, B. L., Van Voorhis, W. C., Myler, P. J. & Stewart, L. J. (2011). *BMC Struct. Biol.* **11**, 39.
Emsley, P. & Cowtan, K. (2004). *Acta Cryst.* D**60**, 2126–2132.
Evans, P. (2006). *Acta Cryst.* D**62**, 72–82.
Evrard, G. X., Langer, G. G., Perrakis, A. & Lamzin, V. S. (2007). *Acta Cryst.* D**63**, 108–117.
Gorrec, F. (2009). *J. Appl. Cryst.* **42**, 1035–1042.
Graille, M., Meyer, P., Leulliot, N., Sorel, I., Janin, J., Van Tilbeurgh, H. & Quevillon-Cheruel, S. (2005). *Biochimie*, **87**, 763–769.
Hamada, K., Ago, H., Sugahara, M., Nodake, Y., Kuramitsu, S. & Miyano, M. (2003). *J. Biol. Chem.* **278**, 49183–49190.
Hargreaves, D. (2012). *J. Appl. Cryst.* **45**, 138–140.
Holmes, M. A. *et al.* (2006). *Acta Cryst.* F**62**, 427–431.
Ishikawa, K., Matsui, I., Payan, F., Cambillau, C., Ishida, H., Kawarabayasi, Y., Kikuchi, H. & Roussel, A. (2002). *Structure*, **10**, 877–886.
Jacquamet, L., Joly, J., Bertoni, A., Charrault, P., Pirocchi, M., Vernede, X., Bouis, F., Borel, F., Périn, J.-P., Denis, T., Rechatin, J.-L. & Ferrer, J.-L. (2009). *J. Synchrotron Rad.* **16**, 14–21.
Jacquamet, L., Ohana, J., Joly, J., Borel, F., Pirocchi, M., Charrault, P., Bertoni, A., Israel-Gouy, P., Carpentier, P., Kozielski, F., Blot, D. & Ferrer, J.-L. (2004). *Structure*, **12**, 1219–1225.
Jung, J., Kim, J.-K., Yeom, S.-J., Ahn, Y.-J., Oh, D.-K. & Kang, L.-W. (2011). *Appl. Microbiol. Biotechnol.* **90**, 517–527.
Keegan, R. M. & Winn, M. D. (2007). *Acta Cryst.* D**63**, 447–457.
Kim, T. G., Kwon, T. H., Min, K., Dong, M.-S., Park, Y. I. & Ban, C. (2009). *Mol. Cells*, **27**, 99–103.
Krissinel, E. & Henrick, K. (2007). *J. Mol. Biol.* **372**, 774–797.
Leslie, A. G. W. (2006). *Acta Cryst.* D**62**, 48–57.
Maire, A. le, Gelin, M., Pochet, S., Hoh, F., Pirocchi, M., Guichou, J.-F., Ferrer, J.-L. & Labesse, G. (2011). *Acta Cryst.* D**67**, 747–755.
Murshudov, G. N., Skubák, P., Lebedev, A. A., Pannu, N. S., Steiner, R. A., Nicholls, R. A., Winn, M. D., Long, F. & Vagin, A. A. (2011). *Acta Cryst.* D**67**, 355–367.
Murzin, A. G., Brenner, S. E., Hubbard, T. & Chothia, C. (1995). *J. Mol. Biol.* **247**, 536–540.
Neville, B. A. & O'Toole, P. W. (2010). *Future Microbiol.* **5**, 759–774.
Nicholls, R. A. (2011). PhD thesis. University of York.
Nichols, C. E., Sainsbury, S., Ren, J., Walter, T. S., Verma, A., Stammers, D. K., Saunders, N. J. & Owens, R. J. (2009). *Acta Cryst.* F**65**, 204–209.
O'Callaghan, J., Buttó, L. F., MacSharry, J., Nally, K. & O'Toole, P. W. (2012). *Appl. Environ. Microbiol.* **78**, 5196–5203.
Ohana, J., Jacquamet, L., Joly, J., Bertoni, A., Taunier, P., Michel, L., Charrault, P., Pirocchi, M., Carpentier, P., Borel, F., Kahn, R. & Ferrer, J.-L. (2004). *J. Appl. Cryst.* **37**, 72–77.
Pearson, W. R. & Lipman, D. J. (1988). *Proc. Natl Acad. Sci. USA*, **85**, 2444–2448.
Pei, J., Kim, B.-H. & Grishin, N. V. (2008). *Nucleic Acids Res.* **36**, 2295–2300.
Rangarajan, E. S., Sivaraman, J., Matte, A. & Cygler, M. (2002). *Proteins*, **48**, 737–740.
Roos, A. K., Andersson, C. E., Bergfors, T., Jacobsson, M., Karlén, A., Unge, T., Jones, T. A. & Mowbray, S. L. (2004). *J. Mol. Biol.* **335**, 799–809.
Roos, A. K., Burgos, E., Ericsson, D. J., Salmon, L. & Mowbray, S. L. (2005). *J. Biol. Chem.* **280**, 6416–6422.
Sauter, N. K., Grosse-Kunstleve, R. W. & Adams, P. D. (2004). *J. Appl. Cryst.* **37**, 399–409.
Stein, N. (2008). *J. Appl. Cryst.* **41**, 641–643.

Stern, A. L., Naworyta, A., Cazzulo, J. J. & Mowbray, S. L. (2011). *FEBS J.* **278**, 793–808.
Strange, R. W., Antonyuk, S. V., Ellis, M. J., Bessho, Y., Kuramitsu, S., Yokoyama, S. & Hasnain, S. S. (2009). *Acta Cryst.* F**65**, 1214–1217.
Studier, F. W. (2005). *Protein Expr. Purif.* **41**, 207–234.
Vagin, A. & Teplyakov, A. (2010). *Acta Cryst.* D**66**, 22–25.
Walter, T. S. *et al.* (2005). *Acta Cryst.* D**61**, 651–657.
Wang, X. *et al.* (2012). *Nature Struct. Mol. Biol.* **19**, 424–429.
Winter, G. (2010). *J. Appl. Cryst.* **43**, 186–190.
Xu, Q. *et al.* (2004). *Proteins*, **56**, 171–175.
Zhang, R., Andersson, C. E., Savchenko, A., Skarina, T., Evdokimova, E., Beasley, S., Arrowsmith, C. H., Edwards, A. M., Joachimiak, A. & Mowbray, S. L. (2003). *Structure*, **11**, 31–42.
Zhang, R. G., Andersson, C. E., Skarina, T., Evdokimova, E., Edwards, A. M., Joachimiak, A., Savchenko, A. & Mowbray, S. L. (2003). *J. Mol. Biol.* **332**, 1083–1094.
Zhang, Z., Sauter, N. K., van den Bedem, H., Snell, G. & Deacon, A. M. (2006). *J. Appl. Cryst.* **39**, 112–119.